Chinese Chemical Letters 34 (2023) 107763

Contents lists available at ScienceDirect

Chinese Chemical Letters

journal homepage: www.elsevier.com/locate/cclet

Fabrication of microwave-sensitized nanospheres of covalent organic framework with apatinib for tumor therapy

Qijun Du[a,c,1], Jian Zou[a,1], Zhongbing Huang[a,*], Shimei Li[a], Longfei Tan[b], Xiangling Ren[b], Guangfu Yin[a], Yongfa Zheng[d,*], Xianwei Meng[b,*]

[a] College of Biomedical Engineering, Sichuan University, Chengdu 610065, China
[b] Laboratory of Controllable Preparation and Application of Nanomaterials, CAS Key Laboratory of Cryogenics, Technical Institute of Physics and Chemistry, Chinese Academy of Sciences, Beijing 100190, China
[c] Sichuan Kangcheng Biotechnology Co., Ltd., Chengdu 610041, China
[d] Department of Oncology, Renmin Hospital of Wuhan University, Wuhan 430060, China

ARTICLE INFO

Article history:
Received 3 April 2022
Revised 16 August 2022
Accepted 17 August 2022
Available online 20 August 2022

Keywords:
Covalent organic framework
Antiangiogenesis
Tumor therapy
Microwave hyperthermia
Hollow spheres

ABSTRACT

A new nanocomposite of hollow covalent organic framework (COF) conjugated with the apatinib (AP) and loading microwave-sensitizer (ionic liquid, IL) was prepared by layer by layer (LBL) method and hyaluronic acid (HA) coating, named as COF-AP-IL@HA. AP loading rate in COF hollow-spheres (~30 nm shell thickness) was ~40.3%, due to the interactions of hydrogen and π-π bonds between AP and COF shell, and acidic environment destroyed COF structure, promoting AP release. Microwave sensitization of loaded IL in COF hollow-spheres could enhance the microwave heat-effect, and combined AP therapeutic ability, leading to their higher inhibitation on tumor, due to targeting ability of HA and the local release of apatinib. 88.9% of inhibition rate of COF-AP-IL@HA under microwave on the *in vivo* tumor was significantly higher than those without microwave (12.3%) and COF-IL@HA with microwave (37.5%), indicating a synergism of sensitized microwave hyperthermia and AP therapy on the reduced expression of VEGF *via* the downregulation pathway of hypoxia inducible factor. These results indicated that COF-AP-IL@HA was potential to the application in the combination therapy of tumor of the sensitized microwave hyperthermia and apatinib.

Liver cancer is one of the main diseases threatening human health [1,2]. Drug chemotherapy, as one of the current main treatment methods, has greatly improved the survival rate of tumor patients. However, its shortcomings still exist, such as bad stability and non-specific release of drugs, leading to systemic toxicity [3]. So, a number of nanomaterials, as drug carriers for efficient delivery, have been developed. Common drug-loaded nano-systems include inorganic carriers [4], organic carriers [5] and metal carriers [6], which have achieved better progress for many clinical examples. However, some defects of these materials still limit their wider application in drug-delivery, such as biological toxicity, difficult degradability, lower loading rate and burst release, leading to their worse therapeutic effect. So the repeated treatment is required, increasing the risk of systemic toxicity and drug resistance of the tumor. Drug molecules are usually simply immersed in the pores of common nano-carriers, such as porous silica, so the worse adsorption interaction between the drug molecules and the pore surface leads to their lower loading rate, poorer transportation of the drug. Therefore, it is still a challenge to explore a carrier with higher efficiency of drug delivery, good biocompatibility and better targeting ability.

Covalent organic frameworks (COFs) are composed of light element atoms connected with strong covalent bonds, so they have the characteristics of low mass density and high thermal stability [7,8]. Recently, COFs have been widely applied in semiconductors [9], carbon dioxide capture [10], storage [11], catalysis [12] and biosensing [13]. Furthermore, the high specific surface area and controllable pore diameter of COFs have also resulted in their application in drug delivery [14–16]. The high nitrogen content in COFs provides a large number of lone pairs of electrons, which can be connected with the loaded drug through hydrogen bonds and π-π bonds, significantly increasing its loading capacity of drug [17]. At the same time, COFs are chemically stable under water and physiological conditions, and there are not toxic metals, metal oxides in COFs and their hydrolysates, so COFs have hardly bio-

* Corresponding authors.
E-mail addresses: 195773820@qq.com, zbhuang@scu.edu.cn (Z. Huang), zyftgwz1986@163.com (Y. Zheng), mengxw@mail.ipc.ac.cn (X. Meng).
[1] These authors contributed equally to this work.

https://doi.org/10.1016/j.cclet.2022.107763
1001-8417/

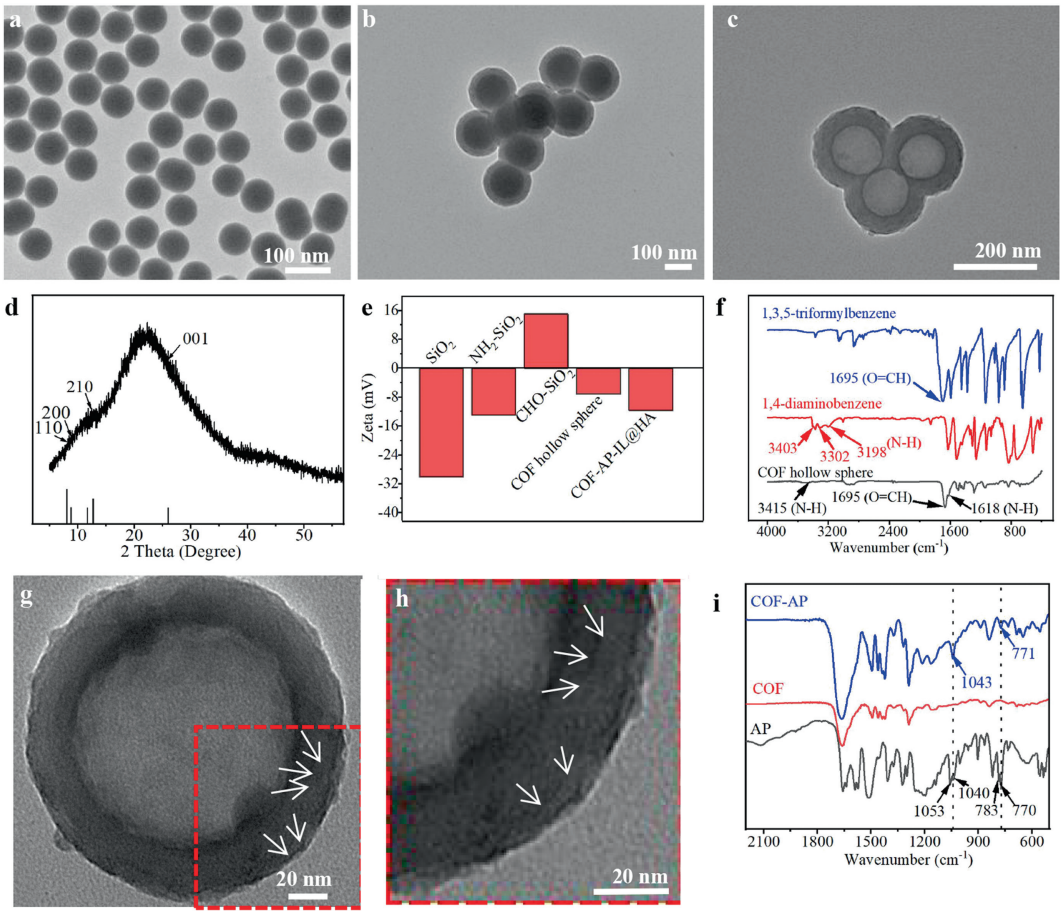

Fig. 1. TEM images of various particles: (a) SiO_2, (b) COF@SiO_2, (c) hollow COF. (d) XRD pattern of hollow spheres. (e) Potential changes of various particles. (f) FTIR spectra of reactants and products. (g, h) TEM images of a magnified hollow sphere. (i) FTIR spectra of hollow COF before/after loading drug.

logical toxicity when degraded in the body, leading to their good application prospects in the biomedicine [18–22]. Hyaluronic acid (HA), a natural glycosaminoglycan with good biocompatibility and degradability, could mediate the targeting recognition of CD44-overexpressed cancer cells [23].

Apatinib (AP), *N*-[4-(1-cyano-cyclopentyl)phenyl]-2-[(4-pyridinylmethyl)amino]-3-picolinamide, is a small molecule tyrosine kinase inhibitor with high selectivity for VEGFR-2, which can limit the activity of key signal molecules in cell VEGFR-2 pathway through dephosphorylation mechanism [24], resulting in the decrease of transcription and expression of downstream signal of HIF-1α molecules and VEGF, thereby effectively preventing tumor angiogenesis [25]. However, apatinib is insoluble and poor stable, so it is very important to develop a stable carrier of apatinib.

Recently, we have prepared COF hollow spheres through LBL method, and obtain ~40% loading rate of doxorubicin drug [26]. In this work, COF nano-spheres with hollow structure were prepared through LBL method, and apatinib were conjugated in COF shell *via* anchoring drug molecules on the free electron pairs of the imine nitrogen of COF, due to non-covalent interactions of π-π bonds [17]. At the same time, the ionic liquid (IL), as a microwave sensitizer, was also loaded in the hollow nano-spheres to enhance their microwave hyperthermia (Fig. S1 in Supporting information). The drug-delivery and microwave sensitization of these COF nanocomposites were analyzed, and their combination of chemotherapy and hyperthermia on tumor *in vitro* and *in vivo* were evaluated.

SEM image in Fig. 1a revealed that, SiO_2 particles were spherical, and their mean size was ~125 nm. As shown in Fig. 1b, it is obvious that a shell layer was formed on SiO_2 surface, and its mean thickness was ~30 nm. Similarly, the particle size distribution from SEM image was shown in Fig. S2 (Supporting information), indicating that their mean particle size was ~188 nm, and the increased particle size corresponded to the shell thickness. TEM image of COF hollow nano-spheres and the size distribution of hollow spheres in Fig. 1c and Fig. S2c (Supporting information) suggested that the alkali corrosion on SiO_2 nano-spheres did not affect the shell structure, the shape and size of hollow nano-spheres.

XRD pattern of COF nano-spheres in Fig. 1d shows that, four obvious peaks of (110), (200), (210) and (001) at 8.13°, 9.02°, 13.01° and 26.06° [27], respectively, suggested the existence of crystal structure of COF. Potential changes of different intermediate products in Fig. 1e showed that, after SiO_2 with the initial potential of –30.1 mV was aminated, the potential of NH_2-SiO_2 was –13.0 mV, indicating the successful linkage of amino groups on SiO_2 surface. During the LBL process, the reaction of NH_2-SiO_2 with the ligand trimesaldehyde led to the positive surface potential of aldehyde-modified particles (CHO-SiO_2, 15.0 mV), and the formation of COF structure on SiO_2 surface resulted in their potential into –7.1 mV, because lots of the imine groups in COF were protonated and absorbed lots of hydroxyl groups with negative charges. Finally, after a layer of negatively charged hyaluronic acid was coated on the surface of the hollow nano-sphere, their surface potential was changed into –11.7 mV. FTIR patterns of the reactants and COF hollow sphere were shown in Fig. 1f. There was a strong C=N tensile vibration peak at 1618 cm^{-1}, indicating the presence of imine bonds in the sample. The peaks at 1695 cm^{-1} and 3415 cm^{-1} of COF hollow nano-sphere corresponded to the absorption

of the terminal aldehyde and amino chemical bonds at the edge of COF spheres, respectively. Compared to the corresponding peaks of trimellitic and *p*-phenylenediamine of the reactants, the peaks of aldehyde groups and amino groups of COF nano-spheres were weakened, due to the formation of the imine bond through the condensation between aldehyde groups and primary amines, indicating the successful formation of COF composition. A TEM and its amplified image in Figs. 1g and h further shows the clear hollow structure of COF, and there were obviously multilayer structure (pointed by black arrows) and many nano-pores in its shell (shown by white arrows), and these pore size was ~3 nm, corresponded with the 2~4 nm of the median pore width *via* N_2 adsorption-desorption curves (Figs. S3a and b in Supporting information). In addition, the cumulative surface area of COF nanospheres *via* N_2 adsorption-desorption method was ~33.2 m^2/g, suggesting that their better median pore size was beneficial to loading and release of drug.

In order to evaluate its pH-response degradation, COF-AP-IL@HA was cultured in PBS (pH 5.7) at 37 °C. After the immersion of 2 h, the spherical skeleton deformed (Fig. S4a in Supporting information), and even the sphere shape disappeared. The immersion of 4 h resulted in the collapse of the spherical skeleton, and those sphere bodies tended to agglomerate together (Fig. S4b in Supporting information). The immersion of 6 h led to the disappearance of the hollow structure, and the random fragments were aggregated together (Fig. S4c in Supporting information). Fig. S5 (Supporting information) shows their corresponding size distribution under different immersion time, and the nano-spheres at 2 h exhibit the size of 200–800 nm and a wide size distribution, indicating that only part of the nano-spheres was degraded and agglomerated. The particle size distribution at 4 h and 6 h tended to be larger, suggesting that the accumulation trend of degraded COF-AP-IL@HA under acidic condition were potential to release the loaded drugs.

According to the method of Fig. S1, the encapsulation efficiency of apatinib in the hollow nano-sphere was ~67.5%, and the drug loading rate of apatinib in COF-AP-IL@HA was up to ~40.5 wt%. FTIR patterns of apatinib and COF-AP in Fig. 1i show that the peaks at 1053 and 1040 cm^{-1} in AP curve were attributed to imino groups of apatinib, however, there was only the existence of the peak at 1043 cm^{-1} in COF-AP pattern, suggesting that many hydrogen bonds between the imino group of apatinib and amino group of COF surface were formed [17], leading to the blue shift of the peak from 1053 cm^{-1} to 1043 cm^{-1}. Similarly, the peaks at 783 and 770 cm^{-1} in AP pattern were attributed to aromatic rings of apatinib, however, there was only the existence of the peak at 771 cm^{-1} in COF-AP curve, suggesting that lots of π-π interactions between the aromatic rings of apatinib and COF surface appeared [1], resulting in the blue shift of the peak from 783 cm^{-1} to 771 cm^{-1}. These results suggested that COF hollow nano-spheres with multilayer structure was beneficial to the apatinib loading *via* hydrogen bonds and π-π interactions of the aromatic rings, significantly enhancing their loading drug rate. To explore the controlled release ability of COF-AP-IL@HA, the drug release of nano-carriers were immersed in two solutions, respectively: (1) acidic buffer solution (pH 5.7), neutral buffer solution (pH 7.2), and their results of drug release were shown in Fig. 2a. Under neutral conditions, the release of apatinib was slow and the release rate at 24 h was only ~41.6 wt%. The release rate under the acidic condition was significantly improved, due to the collapse and destruction of COF nano-spheres, and the final rate of released drug at 24 h reached ~76.3 wt%, suggesting a good pH-responsive drug release of COF-AP-IL@HA.

To evaluate their microwave sensitization, COF-AP-IL@HA nano-spheres were dispersed in 1 mL of PBS with different concentrations of nano-spheres, and then these suspensions were placed under the microwave radiation. The real-time infrared photos of

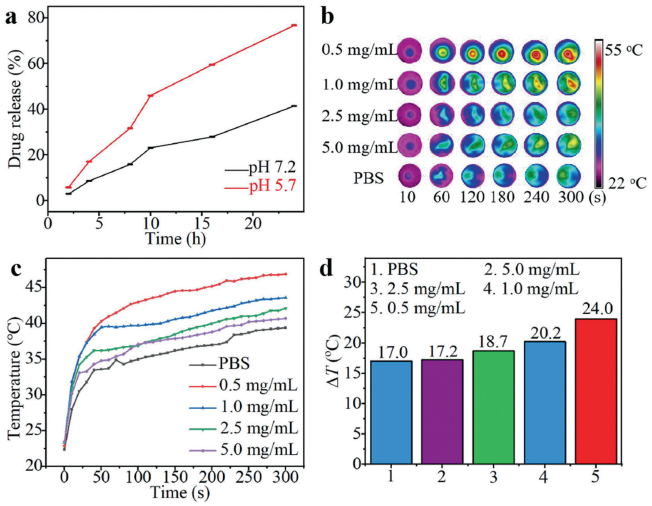

Fig. 2. (a) Apatinib release of COF-AP-IL@HA in PBS with two pH values. Temperature changes of COF-AP-IL@HA suspension with different concentration under MW: (b) infrared thermal images; (c) temperature change curves; (d) heated temperatures; MW irradiation: 1.8 W, 5 min.

these suspensions and their corresponding temperature change were shown in Figs. 2b and c, indicating that the temperature of each experimental group was obviously higher than PBS group. Temperature increase of each group was shown in Fig. 2d, indicating only 16.9 °C of increase in PBS solution, however, the temperature increases of COF-AP-IL@HA suspensions with 1.0 and 0.5 mg/mL concentration were 21.3 °C and 25.0 °C, respectively, indicating the good microwave sensitization of COF-AP-IL@HA. The higher the concentration of COF-AP-IL@HA suspensions, the less the elevated temperature, which results from the reduced probability of ions colloid in higher concentration.

To explore their cyto-compatibility, the cell viability of COF-IL@HA were analysed *via* their co-culture with L929, H22 and HepG2 for 24 h, respectively, and the viability of these cells showed that with the increase of the material concentration, the viability of L929 cells slightly decreased to a certain extent (Fig. S6 in Supporting information); similarly, the viability of H22 cell of the highest material concentration in Fig. 3a was ~80%, even the viability of HepG2 cells at the highest concentration in Fig. 3b was still as high as 98.77%, indicating that COF-IL@HA materials had very low cytotoxicity. Furthermore, it is seen from Fig. 3c that with the concentration increase, the inhibitory effect of COF-AP-IL@HA on HepG2 cells was gradually increased, and the cell viability at the highest concentration of 200 μg/mL was only 66.4%, indicating a certain dose toxicity of COF-AP-IL@HA on HepG2 cells. Hyperspectral images of COF-AP-IL@HA co-cultured with HepG2 cells (Figs. S7c and d in Supporting information) showed that lots of nano-spheres were on cell membrane or inside cell, suggesting the better recognition and endocytosis of COF-AP-IL@HA on tumor cells.

To explore the inhibitory effect of COF-AP-IL@HA under microwave, experiments on H22 cells were further carried out. It is found from Fig. 3d that, after 5 min of microwave irradiation, the cell viabilities of COF-IL@HA + MW group and COF-AP-IL@HA + MW group were significantly decreased, and they reached 65.3% and 52.4%, respectively. Compared with MW group, cell viability of COF-IL@HA + MW group was significantly reduced, indicating a good effect of microwave sensitization of COF-IL@HA and COF-AP-IL@HA, which killed tumor cells much effectively under the same MW irradiation. Due to the co-loading apatinib and IL in COF-AP-IL@HA + microwave group, the higher microwave sensi-

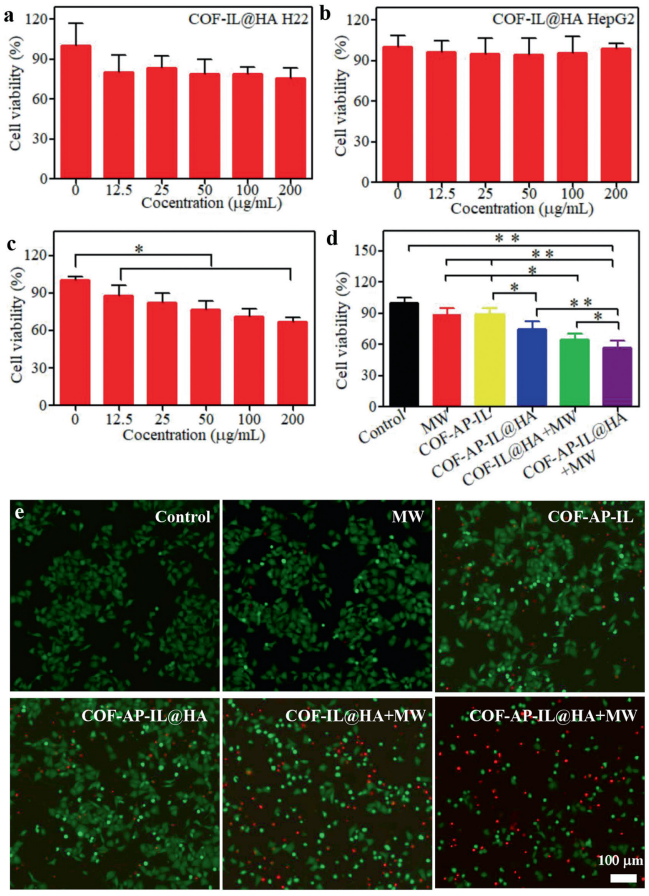

Fig. 3. Cell viability of COF-IL@HA with various concentrations: (a) H22, (b) HepG2, (c) COF-AP-IL@HA on HepG2. (d) Viability of H22 cells under different treatments. (e) Images of stained H22 cell in therapy experiments: green live cells and red dead cell. $^{*}P < 0.05$, and $^{**}P < 0.01$ show significant difference between two corresponding groups.

tization of IL produced effect of better hyperthermia, and the inhibition of apatinib released from the composite nano-spheres much significantly killed tumor cells, indicating their higher therapy effect on tumor. Moreover, it is also found from Fig. 3d that, the cell viability in COF-AP-IL@HA group was ~74.7%, significantly lower than 87.2% of COF-AP-IL group, suggesting the targeting effect of HA and the easy adhesion or entrance of nano-spheres onto/into tumor cells, leading to the apoptosis of more cells. Fluorescence images of stained live and dead cells of different groups after the material or microwave treatments were shown in Fig. 3e and Fig. S8 (Supporting information). It is seen from Fig. S8 that compared with microwave group, COF-AP group only exhibited a slight therapeutic effect; however, dead cells in COF-AP@HA group were more than COF-AP group, suggesting HA targeting ability on tumor cell. Moreover, there were only a small amount of live cells and lots of dead cells in the view field of COF-IL@HA + MW group or COF-AP-IL@HA + MW group, indicating a significant limitation of two treatments on cells.

Animal acute toxicity analyses of COF-IL@HA were performed through (ICR Institute of Cancer Research) mouse. Weight change of mice in 14 days after intravenous injection of different doses of COF-AP-IL@HA was shown in Fig. S9 (Supporting information), and it is found that there was no significant difference in body weight among the different groups. The results of a blood routine analysis were shown in Fig. S10 (Supporting information), including hematocrit (HCT), mean platelet volume (MPV), hemoglobin (HGB), red blood cell count (RBC), mean hemoglobin content (MCH), mean red blood cell volume (MCV), and there was no significant difference between each test group and the control group. The result of blood biochemical analysis of the serum was shown in Fig. S11 (Supporting information), also indicating that there was no significant change between each test group and control group, suggesting the good blood-compatibility of COF-AP-IL@HA. Images of H&E-stained sections of heart, liver, spleen, lung, and kidney tissues of mouse were shown in Fig. S12 (Supporting information), and no obvious abnormal changes were found, indicating that there was no tissue damage from the materials. These results confirmed that a good biological safety of COF-AP-IL@HA composite nano-spheres.

Inhibition effect of COF-IL@HA and COF-AP-IL@HA on tumor growth were evaluated through H22-tumor bearing mice with ~23 g of weight. Under microwave irradiation, the infrared photos and temperature changes of the tumor site were shown in Fig. S13 (Supporting information). After 5 min of microwave irradiation, the temperature of tumor site in microwave group was increased from 37.1 °C to 43.3 °C ($\Delta T = 6.2$ °C); however, the temperature of COF-IL@HA + microwave and COF-AP-IL@HA + microwave groups reached 49.0 °C and 50.0 °C, respectively, and the heating values of the tumor area of the two groups were 11.9 °C and 12.9 °C, respectively, significantly higher than 6.2 °C of MW group. These results indicate that COF-AP-IL@HA significantly promoted the thermal therapy of microwave on tumor, due to the load of IL sensitizers.

In order to research the inhibitory effect *in vivo*, tumor-bearing mice were randomly dividing into control, MW, Apatinib, COF-AP-IL@HA, COF-IL@HA + MW, COF-AP-IL@HA + MW groups, which was approved by the regulations of institutional animal care and use committee of Sichuan Kangcheng Biotechnology Co., Ltd. (No. IACUC-202110-m-007). After the corresponding treatment, the significant difference of the average body weight between each treatment group and the control (Fig. 4a). Tumor volume results in Fig. 4b indicated that, volume change in COF-AP-IL@HA + MW was the smallest among all groups, suggesting the obvious tumor inhibition effect of this treatment. Compared with other treatments, tumor volume changes in COF-AP-IL@HA group showed an obvious inhibition during 19 days ($P < 0.05$ or $P < 0.01$), due to the slow and constant release of the apatinib from the COF composite spheres.

Moreover, the tumor weight growths of MW, Apatinib, COF-AP-IL@HA, COF-IL@HA + MW groups were slower than the control; and the tumor weight of COF-AP-IL@HA + MW was significantly smaller than those of other treatment groups (Fig. 4c). Furthermore, tumor volumes in COF-IL@HA + MW group and COF-AP-IL@HA + MW group at the 19th day decreased significantly, indicating that the microwave sensitizer obviously increased its thermal conversion efficiency of microwave irradiation. Inhibition rate of tumor in COF-AP-IL@HA + MW group was 88.9%, significantly higher than 12.3% of COF-AP-IL@HA group and 37.5% of COF-IL@HA + MW group (Fig. 4d), indicating a better synergism of apatinib release and microwave sensitization. Images of mice and tumor body at the 19th day also further showed that the tumor size in COF-AP-IL@HA + MW group was the smallest (Figs. 4e and f), further suggesting the highest anti-tumor efficiency of this treatment. These results indicated that under the combined action of microwave sensitizers and apatinib, more effective tumor treatment was achieved. In addition, the images of H & E-stained tissue sections of heart, liver, spleen, lung, kidney and tumor in each group in Fig. S14 (Supporting information) showed that, there was no obvious tissue damage in the internal organs of each group, however, large-scale necrosis in the tumor tissues in COF-IL@HA + MW and COF-AP-IL@HA + MW groups could be observed, further indicating that COF-AP-IL@HA with IL sensitizer under MW irradiation could significantly inhibit tumor growth *via* the located hyperthermia *in vivo*.

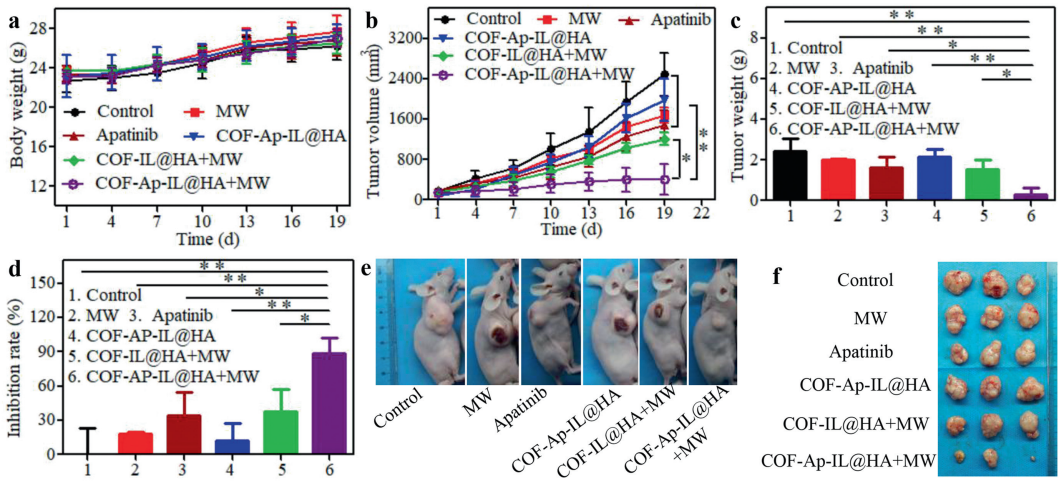

Fig. 4. Therapeutic evaluation of COF-AP-IL@HA *in vivo*. (a) Body weight of HepG2 tumor-bearing mice in each group in 19 days of treatment. (b) Tumor volumes of different groups. (c) Tumor weights of different groups, showing statistically significant difference between COF-AP-IL@HA+MW and other group. (d) Tumor inhibition rates of each group. (e) Representative photographs of mice and (f) tumor tissue from different groups at 19th day post treatment. Statistical analysis: $^{*}P < 0.05$, $^{**}P < 0.01$.

Images of fluorescence-stained HIF-1α and VEGF in Figs. S15 and S16 (Supporting information) showed that, compared to control group, two factors represented by reddish brown objects in tumor tissue of each treatment group gradually decreased. Quantitative results of optical density from these images in Fig. S17a (Supporting information) showed that, amounts of HIF-1α in each treatment were less than control group, because apatinib chemo-effect or MW hyperthermia downregulated HIF-1α secretion. Furthermore, there were the significant decreases of VEGF between each treatment and control (Fig. S17b in Supporting information), and there was similar to changes trend of HIF-1α in each treatment. Amounts in apatinib, COF-AP-IF@HA and COF-AP-IL@HA+MW groups were less than two groups without apatinib (Fig. S17b), further suggesting inhibitation effect of apatinib on angiogenesis HIF-1α secretion in cells significantly limited VEGF generation, *via* inhibition of VEGFR2/phospholipases C (PLC)/Erkl/ERK2 signaling pathway [28].

Based on the above results, the primary mechanism of apatinib chemotherapy and IL-sensitized microwave hyperthermia of COF-AP-IL@HA on cancer were proposed. As shown in Fig. S18a (Supporting information). First, the COF-AP-IL@HA composite nano-spheres were injected into the body of tumor-bearing mice through the tail vein, and then they gradually accumulated in the tumor area through the blood circulation, due to the targeting recognition of HA on CD44 overexpressed by tumor (Fig. S18b in Supporting information) [23]. Some composite nano-spheres were degraded in the acidic condition of tumor area, and slowly released the loaded apatinib, which inhibited the activity of PLC/Erkl/ERK2 signaling pathway in the cellular VEGF2 through a dephosphorylation mechanism, resulting in the reduction of downstream HIF-1α molecule transcription and expression, and thereby inhibiting the downstream vascular endothelial growth factor VEGF [27]; and these results could effectively block the formation of tumor neovascularization, inhibiting tumor cell proliferation (Fig. S18c in Supporting information). On the other hand, under the microwave irradiation, the composite nano-spheres gathered at the tumor site could more efficiently convert microwaves into heat energy, to generate high temperature in the tumor area, killing the tumor cells (Fig. S18d in Supporting information); at the same time, microwave irradiation also led to the re-fracture of the COF structure to release the retained apatinib molecules, further inhibiting the formation of tumor angiogenesis. Therefore, COF-AP-IL@HA realizes the combined effect of tumor chemotherapy and sensitized microwave hyperthermia, thereby inhibiting tumor growth more efficiently.

In this work, COF hollow nanospheres with a shell thickness of ~30 nm were prepared with LBL method; and the apatinib as tumor drug and the ionic liquid as microwave sensitization were co-loaded into them, finally hyaluronic acid was coated on their surface. The loading rate of the apatinib in COF hollow nanospheres was up to 40.5%, due to the hydrogen bonds and π-π bond interactions between apatinib and COF multilayer structure, and acidic environment of simulated tumor could destroyed COF framework, promoting apatinib release. The microwave irradiation for 5 min could heat COF-AP-IL@HA suspension with a concentration of 0.5 mg/mL to increase 24 °C. Cell experiment results showed that coating HA could not only increase cyto-compasibility of COF-IL, but also endow the recognition of COF-AP-IL@HA on HepG2 cells; meanwhile, loading apatinib drug provide a dose toxicity of COF-AP-IL@HA. Although there was better *in vivo* safety of COF-IL@HA at the lower concentrations, COF-AP-IL@HA co-loaded with ionic liquid and apatinib could significantly enhance the inhibitory effect on the *in vivo* tumor under microwave irradiation. 88.9% of inhibition rate of COF-AP-IL@HA under microwave on the *in vivo* tumor was significantly higher than those of COF-AP-IL@HA without microwave (12.3%) and COF-IL@HA with microwave (37.5%), indicating an obvious synergistic effect of apatinib and microwave irradiation. These results indicated that COF-AP-IL@HA could achieved a more efficient tumor inhibition through the clear synergistic effect of sensitized microwave hyperthermia and the chemotherapy of apatinib through a downregulation pathway of HIF-1α and VEGF.

Declaration of competing interest

The authors declare that they have no known competing financial interests or personal relationships that could have appeared to influence the work reported in this paper.

Acknowledgments

This work was supported by the National Key Research and Development Program of China (No. 2018YFC1106800), National Natural Science Foundation of China (No. 81703035), and Sichuan Science & Technology Program (No. 2020YFSY0018).

Supplementary materials

Supplementary material associated with this article can be found, in the online version, at doi:10.1016/j.cclet.2022.107763.

References

[1] Y. Wu, S. Yang, J. Ma, et al., Cancer Discov. 12 (2022) 134–153.
[2] F. Bray, J. Ferlay, I. Soerjomataram, et al., CA-Cancer J. Clin. 68 (2018) 394–424.
[3] O.C. Farokhzad, R. Langer, ACS Nano 3 (2009) 16–20.
[4] Y.Y. Song, F. Schmidt Stein, S. Bauer, P. Schmuki, J. Am. Chem. Soc. 131 (2009) 4230–4232.
[5] S. Sevenson, D.A. Tomalia, Adv. Drug Deliv. Rev. 64 (2012) 102–115.
[6] Z.R. Goddard, M.J. Marin, D.A. Russell, M. Searcey, Chem. Soc. Rev. 49 (2020) 8774–8789.
[7] Z. Kang, Y. Peng, Y. Qian, et al., Chem. Mater. 28 (2016) 1277–1285.
[8] T. Ma, E.A. Kapustin, S.X. Yin, et al., Science 361 (2018) 48–52.
[9] X. Ding, J. Guo, X. Feng, et al., Angew. Chem. Int. Ed. 50 (2011) 1289–1293.
[10] L. Yang, H. Yang, H. Wu, et al., J. Mater. Chem. A 9 (2021) 12636–12643.
[11] H.H. Do, S.Y. Kim, Q.V. Le, N.N. Phamn Tran, Materials 13 (2020) 3322.
[12] S.Y. Ding, J. Gao, Q. Wang, et al., J. Am. Chem. Soc. 133 (2011) 19816–19822.
[13] T. Zhang, N. Ma, A. Ali, et al., Biosens. Bioelectron. 119 (2018) 176–181.
[14] Q. Guan, L.L. Zhou, Y.A. Li, et al., ACS Nano 13 (2019) 13304–13316.
[15] Y. Jia, L. Zhang, B. He, et al., Mat. Sci. Eng. C: Mater. 117 (2020) 111243.
[16] R. Anbazhagan, R. Krishnamoorthi, S. Kumaresan, H.C. Tsai, Mat. Sci. Eng. C: Mater. 120 (2021) 111704.
[17] V.S. Vyas, M. Vishwakarma, I. Moudrakovski, et al., Adv. Mater. 28 (2016) 8749–8754.
[18] S. Feng, M. Yan, Y. Xue, J. Huang, X. Yang, Anal. Chem. 93 (2021) 13572–13579.
[19] A. Modak, A. Ghosh, A.R. Mankar, et al., ACS Sustain. Chem. Eng. 9 (2021) 12431–12460.
[20] X. Yan, Y. Song, J. Liu, et al., Biosens. Bioelectron. 126 (2019) 734–742.
[21] X. Ma, Q. Wu, L. Tan, et al., Chin. Chem. Lett. 33 (2022) 1604–1608.
[22] Y. Lu, J. Xu, Z. Jia, et al., Chin. Chem. Lett. 33 (2022) 1589–1594.
[23] S. Tian, H. Quan, C. Xie, et al., Cancer Sci. 102 (2011) 1374–1380.
[24] S. Hiscox, B. Baruha, C. Smith, et al., BMC Cancer 12 (2012) 458.
[25] M. Li, H. Xie, Y. Liu, et al., J. Control. Rel. 304 (2019) 204–215.
[26] J. Zou, X. Ren, L. Tan, et al., Front. Mater. Sci. 15 (2021) 465–470.
[27] C. Hu, L. Cai, S. Liu, M. Pang, Chem. Comm. 55 (2019) 9164–9167.
[28] T. Mathew, S.K.S. Sarada, Resp. Physiol. Neurobio. 258 (2018) 12–24.